Eos, Transactions, American Geophysical Union, Vol. 76, No. 16, April 18, 1995 Page 161, 164-165

Wavelet Analysis Provides a New Tool for Studying Earth's Rotation

Benjamin Fong Chao and Isao Naito

The solid Earth's rotation varies slightly with time due to geophysical processes that involve motions and redistributions of mass occurring on or within the Earth, as dictated by the conservation of angular momentum. In particular, these variations (ΔLOD) in the atmosphere in terms of the axial atmospheric anglar momentum (AAM) are the primary cause for nontidal length-of-day variations on timescales of several days to several years [e.g., *Rosen*, 1993]. Here ΔLOD is a convenient measure of Earth's rotational speed relative to the uniform time kept by atomic clocks.

AAM and ΔLOD have many periodic oscillations that are more or less stationary in time, such as the seasonal terms with annual and semiannual periods. ΔLOD, in addition, has large tidal terms due to tidal deformations (see below). These are externally forced oscillations with known fixed periods. The Fourier spectrum is a conventional technique for analyzing such periodicities.

But nonstationary oscillations also abound in AAM and hence are duly reflected in ΔLOD. These oscillations could be internal modes that result from couplings between the atmosphere and oceans that evolve with time in amplitude, period, and/or phase. To reveal nonstationary, "localized" periodicities in a time series, the wavelet time-frequency spectrum has proven a powerful tool. A recently developed mathematical technique, wavelet analysis, can be used to represent functions that are local in time and frequency [*Morlet et al.*, 1982]. It has found applications in a wide variety of fields such as speech and signal analysis, image processing, and geophysics. *Gambis* [1992] and *Abarca del Rio and Cazenave* [1994] have used wavelet transform to study some aspects of the interseasonal Earth rotation variations. Here we employ wavelet analysis on two independent data sets and compare them: the geodetically determined LOD variation and the meteorologically derived AAM variation. Their wavelet spectra are shown in Figure 1 (detailed discussion later). They reveal interesting temporal evolution of quasi-periodic and intermittent oscillations in both LOD and AAM, and demonstrate the time-frequency characteristics of the LOD-AAM correlation.

Benjamin Fong Chao, Geodynamics Branch, NASA Goddard Space Flight Center, Greenbelt, MD 20771; and Isao Naito, National Astronomical Observatory, Mizusawa, 023 Japan

Wavelet Time-Frequency Spectrum

The wavelet transform of the time series f(t) is defined as

$$W_\psi(f)(a,b) = \frac{1}{\sqrt{a}} \int_{-\infty}^{\infty} f(t)\, \psi\left(\frac{t-b}{a}\right) dt$$

where $\psi(t)$ is the basic wavelet (or a "wave packet") with effective length that is usually much shorter than the target time series $f(t)$. The variables are a and b: a is the dilation/compression scale factor that determines the characteristic frequency so that varying a gives rise to a "spectrum"; and b is the translation in time so that varying b represents the "sliding" of the wavelet over $f(t)$. The wavelet spectrum is thus customarily displayed in the time-frequency domain, or the a-b space with the horizontal time axis b and the vertical frequency axis a. Orthogonal sets of $\psi(t\text{-}b)/a$ (when a varies in powers of 2 or "octave") are often exploited in applications involving inverse transforms and reconstruction of signals. For our application we select the Morlet wavelet [*Morlet et al.*, 1982], which is a normalized, Gaussian-enveloped complex sinusoid with zero mean. It is only nearly orthogonal but offers satisfactory resolution and stability. We choose to examine the real part of the wavelet transform (for real f). It gives the amplitude undulation with the appropriate polarity and phase with respect to time owing to the symmetric nature of the real part of the Morlet wavelet as the kernel in integral (1). In contrast, the imaginary part, being antisymmetric in the kernel, gives the amplitude undulation as well but imparts a 90° phase shift in time. In many applications the modulus—combining real and imaginary parts—is preferred; but then the polarity/phase information, which is important in the present study, becomes absent. We use color contours such that amplitude peaks and troughs in horizontal successions in high contrast colors indicate the presence of strong oscillations in the data, relative to the weaker and less significant "background" of low color contrast.

Some limitations of the wavelet spectrum should be pointed out: Because of the temporal localization of the wavelet, the frequency resolution is limited. We show resolution at a quarter octave; the nonorthogonality of wavelets within an octave prevents much finer resolutions. Further, the limited time span introduces edge effect to the spectrum, which is more severe with longer periods. In our computation, time series values outside our time span are simply assumed to be zero.

ΔLOD Wavelet Spectrum

Figure 2a shows the geodetically determined ΔLOD derived from the "Space93" data set (courtesy of R. S. Gross, 1994). The data are very rich in signal content: the decadal, seasonal, and long-period tidal signals are the most prominent, superimposed on broad-band interannual and intraseasonal variations.

We shall first remove the decadal and the seasonal signals from the LOD series. The decadal fluctuation (including the mean value), believed to reflect fluid core activities, would be beset by edge effects while little further information than that already evident in Figure 2a would be obtained from the spectrum anyway. The seasonal signal, although interesting in its own right, is not to be studied here. We achieve the removal by performing a simultaneous least-squares fit of these signals to the entire LOD series followed by subtraction (decadal signal represented by a fourth degree polynomial and seasonal signals by annual and semiannual sinusoids). A year-by-year empirical removal of the seasonal terms is not desirable here, as signals at nearby periods would be removed because of the limited spectral resolution of the yearly series and the adaptive nature of the fitting procedure.

Figure 1a displays the wavelet spectrum of the resultant nonseasonal ΔLOD series within the frequency range corresponding to periods of 6.25 days to 3200 days. The short-period cutoff was chosen because of the inherent smoothing of the Space93 LOD data at several days. The long-period cutoff was selected because the spectral values at periods longer than that would not be realistic subject to the edge effect.

Toward the top of Figure 2a are the strong long-period tidal signals. Unrelated to the atmosphere, these signals in ΔLOD primarily result from tidal deformations in the solid Earth and are modified by the oceanic tides. The fortnightly zonal tides (primary periods: 13.63, 13.66, and 14.77 days) are rather prominent, with the half-year and 18.6-year modula-

0096/3941/7616/95/161/$01.00.

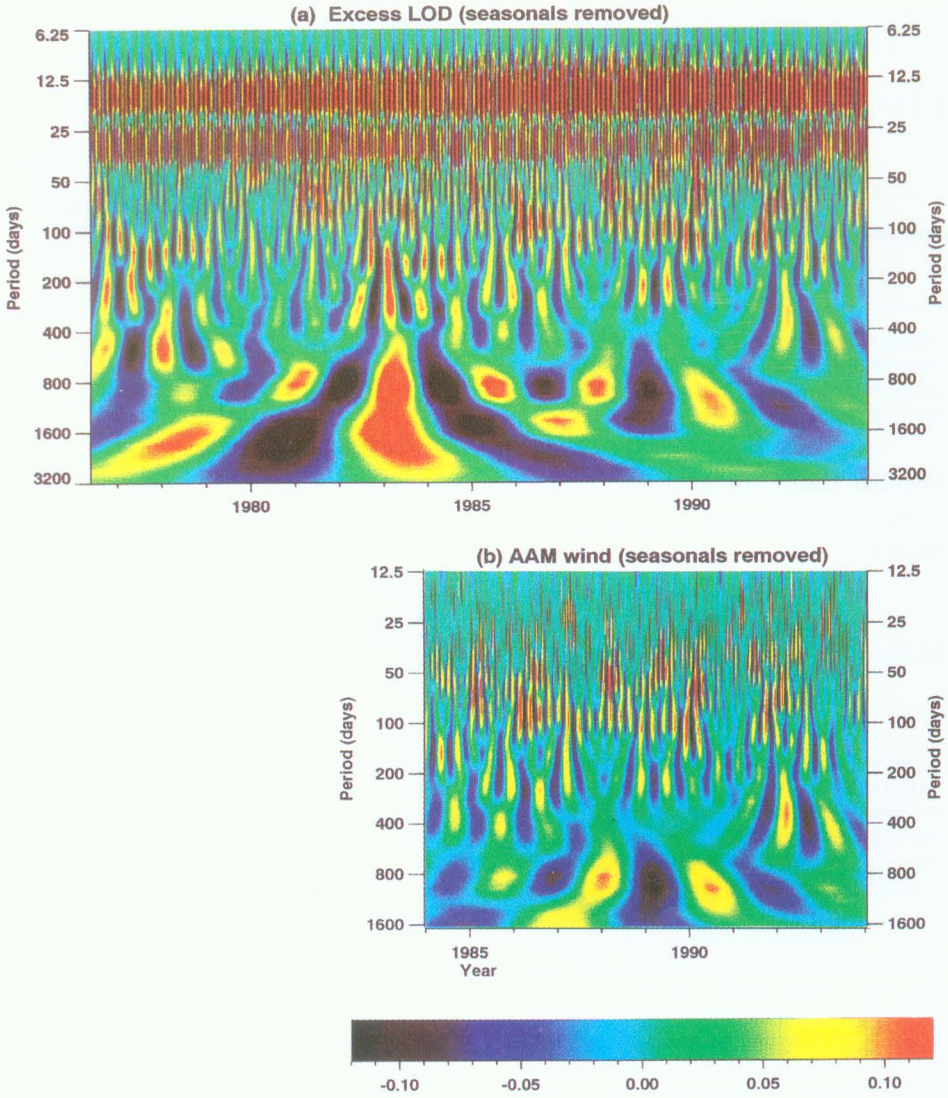

Fig. 1. (a) The wavelet time-frequency spectrum of the nonseasonal version of Figure 2a (ΔLOD after the removal of decadal and seasonal signals). The real part of the spectrum is plotted to show the amplitude undulation with the appropriate polarity and phase with respect to time. (b) The wavelet spectrum of the second curve in Figure 2b, that is, the nonseasonal "wind" term of AAM. Except for the tidal signals, its similarity with (a) on a same scale is evident. Typical extreme amplitudes are <0.18 ms occurring during certain episodes of the 30–60 day oscillation. The color scheme is made to "saturate" beyond the (somewhat arbitrarily selected) spectral amplitude of >0.12 ms to accentuate the significant oscillations in the data.

tion clearly visible. The same is true for the monthly tides (primary periods: 27.55 and 31.81 days) with a somewhat more complex modulation pattern. These and other long-period tidal signals have been well studied using Fourier techniques. The wavelet spectrum offers an interesting way to display the time evolution of the signals, although only the strongest ones can be detected this way.

A more interesting feature appears in the bottom portion of Figure 2a, pertaining to the El Niño/Southern Oscillation (ENSO), which occurs in the tropical Pacific-Indian Ocean region in the troposphere, and the quasi-biennial oscillation (QBO) which occurs in the tropical stratosphere. Their influence on LOD has been demonstrated by *Chao* [1989]. Here we see their oscillatory patterns as a function of time. The QBO stays more or less stationary throughout the studied period at a period of about 800 days (barring the edge effect). On the other hand, ENSO's effect on LOD, where positive polarity indicates El Niño episodes and negative polarity indicates non-El Niño years or La Niña episodes, has periodicity that drifts with time: In the late 1970s and early 1980s, it has a period of about 5 years. During the late 1980s, ENSO seemingly began to bifurcate in period. One strand gradually decreases in period and eventually converges with QBO. The other strand seems to undergo an elongation in period coming into the 1990s, but the detail is unclear due to the edge effect and awaits further data to resolve. This behavior seems consistent with the bimodal behavior of ENSO proposed by *Dickey et al.* [1992].

It is interesting to note that at least during the period studied, there appears to be a phase relation between ENSO and QBO that coincides with the strength of the ENSO phenomenon. The 1982–1983 El Niño event, the strongest on record, occurred when the ENSO and QBO oscillations in ΔLOD were clearly in phase with positive polarity. The subsequent time when the two oscillations were again in phase but with the negative polarity marks the time for the strong 1988–1989 La Niña. The rather mild 1986–1987 El Niño that occurred between these two events occurred when the two oscillations were out of phase. Similarly, the mild 1991–1992 El Niño occurred when the QBO had the negative polarity and hence was again out of phase with ENSO.

AAM Wavelet Spectrum

Let us now study other prominent signals in the ΔLOD series in conjunction with AAM. For the latter, we use the AAM computed by the Japan Meteorological Agency (JMA) (courtesy of T. Ozaki, 1994). The JMA data integrate winds from surface up to the 10-mbar level (altitude of about 30 km), accounting for 99% of the atmosphere in terms of mass. Comparable AAM data sets are available from other meteorological agencies extending a few years farther back in time. They are, however, less homogeneous due to substantial changes in the general circulation models used to assimilate the original meteorological observations. Further, earlier data generally have less complete coverage in altitude, often leaving out the entire stratosphere or a large portion thereof.

Figure 2b gives the "cleaned" series spanning the 10 years of the JMA series, 1984–1993. Similar to the above, the decadal and seasonal LOD variations are removed using the least-squares procedure. Further, tidal variations, represented by 27 major tidal sinusoids, are also removed from LOD. The corresponding nonseasonal AAM series are similarly obtained by removing a mean and the seasonal terms. The AAM values have been converted into equivalent LOD according to *Barnes et al.'s* [1983] formula for the conservation of angular momentum, assuming a complete core-mantle decoupling

and adopting a degree-2 load Love number of -0.30 to account for the solid Earth's elastic yielding effect. The curve labeled "AAM-wind" is the nonseasonal AAM variation due to the global zonal wind field; a small error remains in this term as a result of the exclusion of the part of the stratosphere above 10-mbar level. As expected, its resemblance to the LOD curve is obvious, both showing, in particular, a pronounced La Niña signal in 1988-1989.

The bottom two curves in Figure 2b are the nonseasonal AAM due to the global pressure field assuming either non-IB or IB conditions. IB stands for the inverted-barometer effect, an idealized assumption wherein the ocean would respond to overlying barometric loading in an instantaneous, isostatic manner. Non-IB is the other idealized extreme where the ocean, as if rigid, would simply ignore any atmospheric loading. The total AAM is thus either "wind + pressure" for the non-IB case, or "wind + pressure IB" for the IB case, whereas the reality presumably resides somewhere in between, depending on the temporal and spatial scales of the phenomenon in question. In either case the pressure term only represents a small contribution to the AAM.

Figure 1b shows the wavelet spectrum of the nonseasonal AAM wind term, with a narrower period range than Figure 1a. The shorter long-period cutoff of 1600 days reflects the shorter record time span, and there is little coherent energy in AAM at periods shorter than 12.5 days. Again, the resemblance between Figures 1a and 1b is rather striking, except for the tidal bands in Figure 2a. We do not show the spectra for the total AAM (IB or non-IB); their difference from Figure 1b is hardly discernible simply because of the small amplitude of the added pressure terms and the lack of coherent energy therein (see Figure 2b).

At periods ranging from 30 to 60 days one finds in both ΔLOD and AAM prominent transients with fluctuating strength, period, and phase, typically lasting 5–7 cycles. This is the 30–60 day oscillation, which is sometimes called 40–50 day oscillation. Many studies have been conducted on its possible con nections with atmospheric phenomena with similar periodicities, such as the Madden-Julian oscillation or the instability oscillation in the subtropical winds [e.g., *Eubanks*, 1993]. The wavelet spectra here clearly exhibit the characteristics and the evolution of this oscillation.

AAM variations with periods roughly from 80 to 100 days occur occasionally, presumably representing the evolution of the quarter-year harmonic of the seasonal variation. It appears strongest and fairly coherent during 1986–1990; but the source region and mechanism are presently unidentified. Similar signals appear centered around terannual,

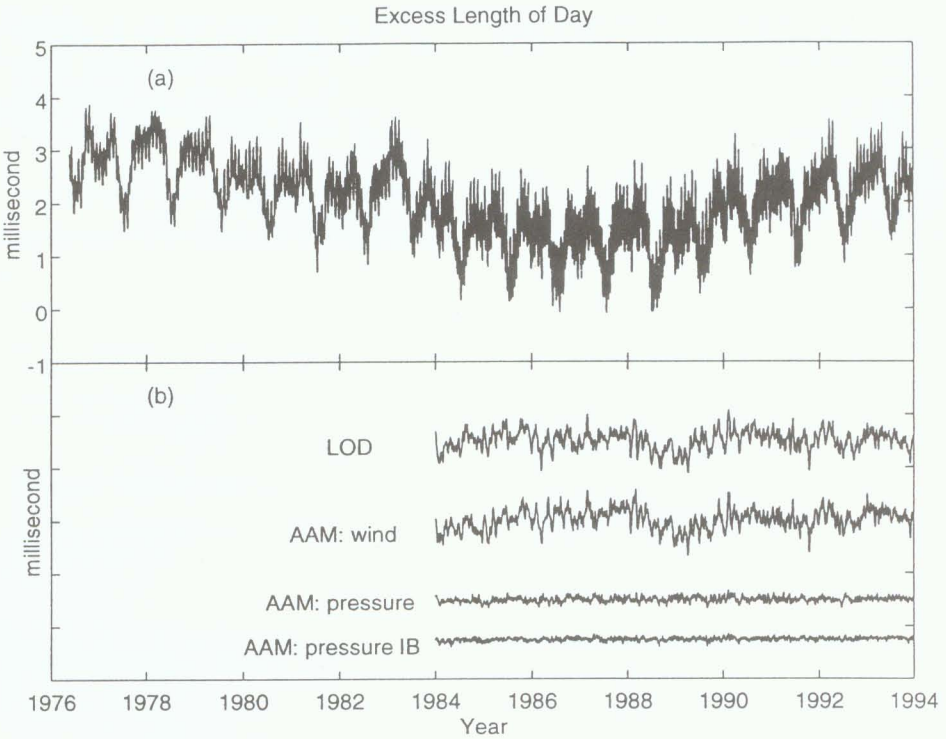

Fig. 2. (a) The geodetically determined daily series of excess length-of-day (ΔLOD, relative to 86400s) over 1976/5/20.0 - 1994/1/9.0. (b) The top curve is the "cleaned" ΔLOD series for 10 years 1984/1/1.0 - 1993/12/31.0, after the removal of the decadal (including the mean), the long-period tidal, and the seasonal signals. The other three curves are the corresponding axial atmospheric angular momentum (AAM) variations after removal of the mean and the seasonal signals, for the "wind" term, the "pressure" term, and the "pressure IB (inverted barometer)" term. They are computed using Japan Meteorological Agency data and have been converted into the equivalent ΔLOD and plotted on the same scale as Figure 2a but shifted vertically.

semiannual and annual periods. These are evidently the residual signals that remain after the overall least-squares removal of the seasonal terms as above. They manifest the year-to-year differences in the seasonal amplitudes and/or phases. One also finds intermittent signal at periods roughly between 200 and 240 days. This coincides with the quasi-7-month oscillation (QSO) first reported by *Naito and Kikuchi* [1992]. The occurrence of this oscillation appears to be related to ENSO: As seen in Figure 1a, QSO appeared during the 1976–1977 El Niño, and again during the 1982–1983 El Niño although the corresponding spectrum covering this period is partially obscured by the semiannual and annual remnants. It became weakest during the 1986-87 El Niño, strongest during the 1988–1989 La Niña, and again disappeared during the El Niño years of 1991–1993. This suggests a meteorological connection between the QSO and ENSO, although a 6-year modulation that controls QSO cannot be ruled out at present. Finally, we mention that the wavelet analysis can be exploited in further detailed studies in terms of latitude zones and altitude layers. This will shed light on the source region and mechanism of the AAM oscillations as well as possible interactions among them.

Acknowledgments

A. A. Liu and C. Y. Peng provided the original wavelet algorithm, and H-T. J. Wu, H. Y. Weng and W. K. M. Lau helped with initial computations. We also thank J. Roark and D. Steinberg for graphic support, R. Gross for providing the Space93 series and the Japan Meteorological Agency for the AAM data. The study is supported by the NASA Geophysics Program and the National Astronomical Observatory of Japan.

References

Abarca del Rio, R., and A. Cazenave, Interannual variations in the Earth's polar motion for 1963–1991: Comparison with atmospheric angular momentum over 1980–1991, *Geophys. Res. Lett., 21*, 2361, 1994.

Barnes, R. T. H., R. Hide, A. A. White, and C. A. Wilson, Atmospheric angular momentum fluctuations, length-of-day changes and polar motion, *Proc. Royal Soc. London, A 387*, 31, 1983.

Chao, B. F., Length-of-day variations caused by El Niño-Southern Oscillation and Quasi-Biennial Oscillation, *Science, 243*, 923, 1989.

Dickey, J. O., S. L. Marcus, and R. Hide, Global propagation of interannual fluctuations in atmospheric angular momentum, *Nature, 357*, 485, 1992.

Eubanks, T. M., Variations in the orientation of the Earth, in *Contributions of Space Geodesy to Geodynamics: Earth Dynamics*, edited by D. E. Smith and D. L. Turcott, pp. 1–54, AGU, Washington, D.C., 1993.

Gambis, D., Wavelet transform analysis of the length of the day and the El Niño/Southern Oscillation variations at intraseasonal and interannual time scales, *Ann. Geophys., 10*, 429, 1992.

Morlet, J., G. Arehs, I. Fourgeau, and D. Giard, Wave propagation and sampling theory, *Geophysics, 47*, 203, 1982.

Munk, W. H., and G. J. F. MacDonald, *The Rotation of the Earth*, Cambridge University Press, New York, 1960.

Naito, I., and N. Kikuchi, Atmospheric contributions to non-seasonal variations in the length of day, *Geophys. Res. Lett., 19*, 1843, 1992.

Rosen, R. D., the axial momentum balance on Earth and its fluid envelope, *Surveys Geophys., 14*, 1–129, 1993.